Proceedings of the ASME 2020
14th International Conference on Energy Sustainability
ES2020
June 8-10, 2020, Denver, CO, USA

DRAFT-ES2020-1687

HIGH-TEMPERATURE THERMOPHYSICAL PROPERTY MEASUREMENT OF PROPOSED GEN3 CSP CONTAINMENT MATERIALS

Sonja A. Brankovic, Bettina Arkhurst, Andrey Gunawan, Shannon K. Yee

Georgia Institute of Technology, Atlanta, GA, USA

ABSTRACT

The US Department of Energy (DOE) has sponsored an initiative to improve the thermal efficiency of Concentrating Solar Power (CSP) systems. To approach parity with conventional fossil fuel-based electricity generation, the operating temperature of the CSP power cycle must exceed 700°C with integrated thermal energy storage. The materials used to house this high-temperature heat transfer media must be thermally stable and corrosion resistant. However, the temperature-dependent thermophysical properties of commonly used containment materials (nickel alloys, alumina-based firebricks, and ceramic metals) are either not well known or poorly understood. In this report, the high-temperature thermal properties of sixteen candidate containment materials proposed by the CSP community are tested using laser flash analysis and differential scanning calorimetry.

Keywords: Concentrating Solar Power (CSP), thermophysical properties, containment materials, thermal metrology, high-temperature material properties

NOMENCLATURE

$c_{p,\,sample}$	Sample specific heat
$c_{p,\,stand}$	Reference specific heat
m_{sample}	Sample mass
m_{stand}	Mass of standard
ΔV_{sample}	DSC signal difference between reference and sample
ΔV_{stand}	DSC signal difference between reference and standard
L	Sample thickness
$t_{1/2}$	Time it takes top-side of sample to reach half the maximum temperature

INTRODUCTION

Concentrating Solar Power (CSP) is a promising alternative to fossil fuel power generation systems. In CSP systems, a concentric field of mirrors focuses sunlight onto a receiving tower. Cold heat transfer media (HTM) is heated by the concentrated sunlight; the heated media is then either stored in a hot tank or used to exchange heat with the working fluid of the attached power block (Fig. 1).

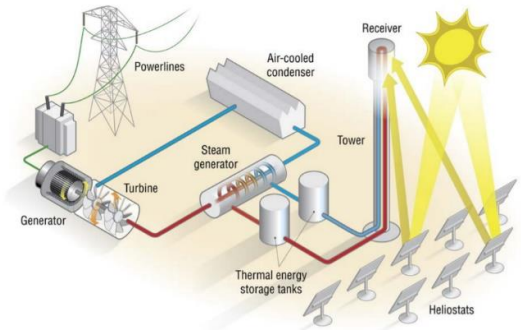

Figure 1: Schematic of Concentrating Solar Power system. Containment materials are used in piping, heat exchangers, and as tank walls [1].

Table 1: Material classification and properties of the candidate containment materials tested for this report. References for density and melting point values are noted in the third column. The top 13 materials were acquired from commercial contacts, while the cermets were sourced from either the Sandhage group at Purdue or Powdermet Inc. Three of these materials did not have published melting temperatures. The density values with stars next to them were measured by the STEEL group at Georgia Tech.

Material classification		Containment material	Density from literature (g/cc)	Melting/maximum operating temperature from literature (°C)
Metal alloys	Austenitic stainless steels	SS 310[2]	8.00	1400-1450
		SS 316[3]	7.90	1390-1440
	Nickel-based alloys	Inconel 740H[4]	8.05	1288-1362
		Inconel 625[5]	8.44	1290-1350
		Haynes 230[6]	8.97	1301-1371
		Haynes 233[7]	8.18	1328-1389
		Haynes HR120[8]	8.07	1300
		Hastelloy N[9]	8.86	1300-1400
Ceramics	Technical ceramics	Graphite[10]	1.30-1.95	3650
		Pyrolytic Boron Nitride (PBN)[11]	2.15-2.19	2973
	Alumina- and silica-based refractories	SR-99 firebrick[12]	3.09	2016
		WAMBLG[13]	2.51	1871
		Durrath HD-45 fireclay[14]	2.40	1800
Ceramic metals (cermets)	Zirconium carbide cermets	ZrC/Mo[15]	8.64 ± .08*	-
		ZrC/W[15]	12.00 ± .16*	2800
	Tungsten carbide cermets	$NiWC_3$[16]	12.40 ± .27*	-
		WC/Cu[15]	10.8-12.3	-

Recently, the DOE has supported several projects – at both the academic and commercial level – to increase the operating temperature of HTM to >700°C and improve long-term energy storage, thereby increasing thermal efficiency and decreasing system costs [17]. However, piping and tank storage materials capable of withstanding high-temperature media such as molten salts or silica-based particles must be carefully selected for temperature and corrosion resistance. The CSP community has suggested several candidate materials, including nickel superalloys, alumina-silica ceramics, and ceramic metals (Table 1 and Figure 2). Since these containment materials will experience a large range of temperatures as heat is exchanged and transferred throughout the system, understanding their temperature-dependent thermophysical properties is key to predicting long-term performance. However, these properties are not well known or understood for these candidate materials.

To investigate these temperature-dependent properties, we measured each sample's thermal diffusivity and specific heat using the laser flash method and differential scanning calorimetry, respectively. This study forms the foundation for understanding the basic thermal properties of containment materials, which span from disordered metal alloys to ceramics embedded in metal matrices.

METHODS

A Netzsch STA 449 F3 Jupiter (Figure 3B) is used to measure temperature-dependent specific heat of the CMs. An STA (Simultaneous Thermal Analyzers) is composed of a Differential Scanning Calorimeter (DSC) and Thermogravimetric Analyzer (TG). Briefly, this tool measures a material's specific heat by comparing the differential amount of heat applied to an empty crucible and a sample-containing crucible to maintain a constant temperature across the crucibles

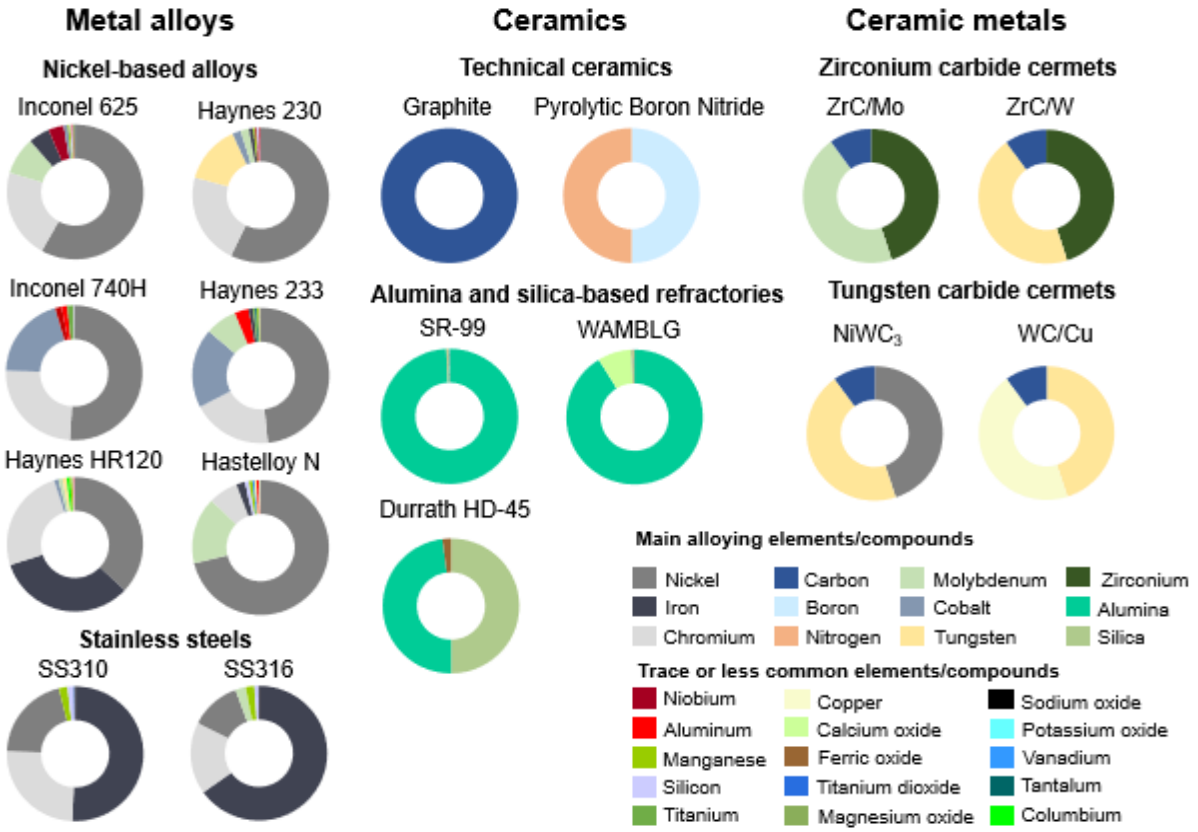

Figure 2: 17 Containment Materials (CMs) proposed for testing by the CSP community. The cermets do not have published compositions; these four were acquired either from the Sandhage group at Purdue University or Powdermet, Inc., an advanced materials contractor. Powdermet has reported that the metal-ceramic volumetric composition of $NiWC_3$ is approximately 40-60, respectively [16].

(Figure 3A). The DSC sensor with the crucibles is encased in an inert chamber surrounded by a 1200°C platinum furnace. Beneath the sensor, a TG balance monitors the sample's mass as it is heated.

For the experiments conducted in this report, three runs with identical temperature profiles and ramp rates (20°C/min) were performed to complete a specific heat measurement: a baseline run with two empty crucibles, a reference run with one empty crucible and one standard material-filled crucible (sapphire), and the final sample run with one empty crucible and the other with the sample. These runs are performed under argon flow (50ml/min purge gas flow rate, 20ml/min protective gas flow rate). Prior to each run, a vacuum is pulled in the chamber and argon is backfilled twice to reduce oxygen content in the system. Once the runs are completed, specific heat is calculated using Netzsch's Proteus software via the ratio method [18]:

$$c_{p,sample}(T) = \frac{m_{stand}}{m_{sample}} \frac{\Delta V_{sample}(T)}{\Delta V_{stand}(T)} \cdot c_{p,stand}(T) \qquad (1)$$

Data acquired from the STA was rejected if the TG signal showed a mass loss of ≥0.3%, as recommended by ASTM E 1269-05 [19]. Thermal diffusivity measurements are made with a Netzsch LFA 467 HT Hyperflash (Figure 3D) at Georgia Tech and Netzsch's testing facility in Boston, MA. The Laser Flash Analyzer (LFA) has a chamber composed of four platinum-furnace encased holders that expose both the bottom and top of the graphite-coated sample. The graphite coating promotes uniform heat absorption. A xenon lamp flashes the samples when they have been heated to the desired temperature; on the opposite side of the sample, a liquid-nitrogen cooled infrared (IR) detector measures the temperature change that occurs over a set time (Figure 3C). The resulting signal versus time "thermogram", is fitted to the Parker (1961) model, which assumes the lamp pulse was absorbed instantaneously and uniformly across the bottom of the sample [20]. Thermal diffusivity α at each temperature is then calculated from this equation:

$$\alpha = \frac{1.38L^2}{\pi^2 t_{1/2}} \quad (2)$$

Sixteen materials are tested and analyzed for this project: SR-99 (Morgan Advanced Materials, Augusta, GA), WAM-BLG (Westmoreland Advanced Materials, Charleroi, PA), Haynes 230 (Haynes Intl, Windsor, CT), Haynes 233 (Haynes Intl, Windsor, CT), Haynes HR120 (Haynes Intl, Windsor, CT), SS310 (Mega Mex, Humble, TX), SS316 (McMaster-Carr, Douglasville, GA), Hastelloy N (Kam Specialties, Inc, Pompano Beach, FL), Inconel 625 (Magellan Metals, Norwalk, CT), Inconel 740H (Special Metals, Huntington, WV), Pyrolytic Boron Nitride (PBN) (MTI Corporation, Richmond, CA), HD45 (Rath Inc., Milledgeville, GA), graphite (Ohio Carbon, Ashland, OH), $NiWC_3$ (Powdermet, Euclid, OH), WC/Cu (Prof. Sandhage's group, Purdue University), ZrC/Mo (Prof. Sandhage's group, Purdue University), and ZrC/W (Prof. Sandhage's group, Purdue University) [2-16].

RESULTS

Specific heat measurements from the STA experiments are shown in Figure 4A. At the time of writing, five of the containment materials have been tested; two of the nickel-based alloys (Haynes 230 and 233), two alumina-silica firebricks (WAMBLG and SR99), and one cermet (WC/Cu). The two Haynes alloys show distinct second-order phase changes starting at ~600°C, while the other materials show only modest, linear increases in specific heat over the tested temperature range. Robust measurements on the STA have been confounded by sample oxidation (particularly in the nickel-based alloys), sintering of the sample to the platinum crucibles at high temperatures, and inconsistencies in pre-annealing samples.

Oxidation issues are detected by the TG balance; an increase of even 0.5% of the initial mass can cause the specific heat to artificially decrease in high-nickel content samples. Samples often visually darken with an oxidation layer as well. To counter this, pre-testing sample preparation procedures such as annealing within the STA or an argon-filled glovebox are being explored.

Figure 4B shows the temperature-dependent thermal diffusivity results for the sixteen containment materials. At each temperature, the samples are flashed three times; the graph displays the average of these three flashes. Measurement uncertainty is displayed as bands above and below each nominal value. Aside from graphite and one of the cermets (WC/Cu), the measured diffusivities remain relatively constant over the tested temperature range. The curves of the nickel-based alloys appear to collapse on each other at high temperatures.

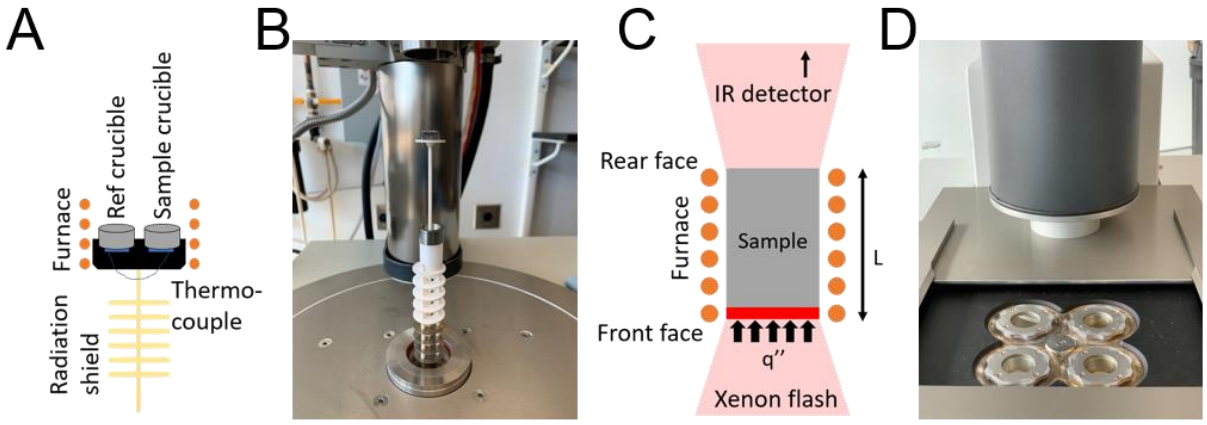

Figure 3: **A**. Schematic of a heat-flux Differential Scanning Calorimeter (DSC). **B**. Image of Netzsch STA 449 F3 Jupiter. The DSC sensor is protected by a series of ceramic plates. A zirconium getter ring is placed on top of the plates to absorb any oxygen that remains in the system after two vacuum evacuations. **C**. Schematic of Laser Flash Analyzer (LFA). Heat from the xenon lamp flash is absorbed uniformly and instantaneously absorbed by the bottom of the sample (red section). **D**. Netzsch LFA 467 HT Hyperflash. Four small chambers can hold 10-12.7mm diameter sample disks. The liquid nitrogen-cooled IR detector is the cylinder above the samples and the xenon lamp is located below the chambers within the machine.

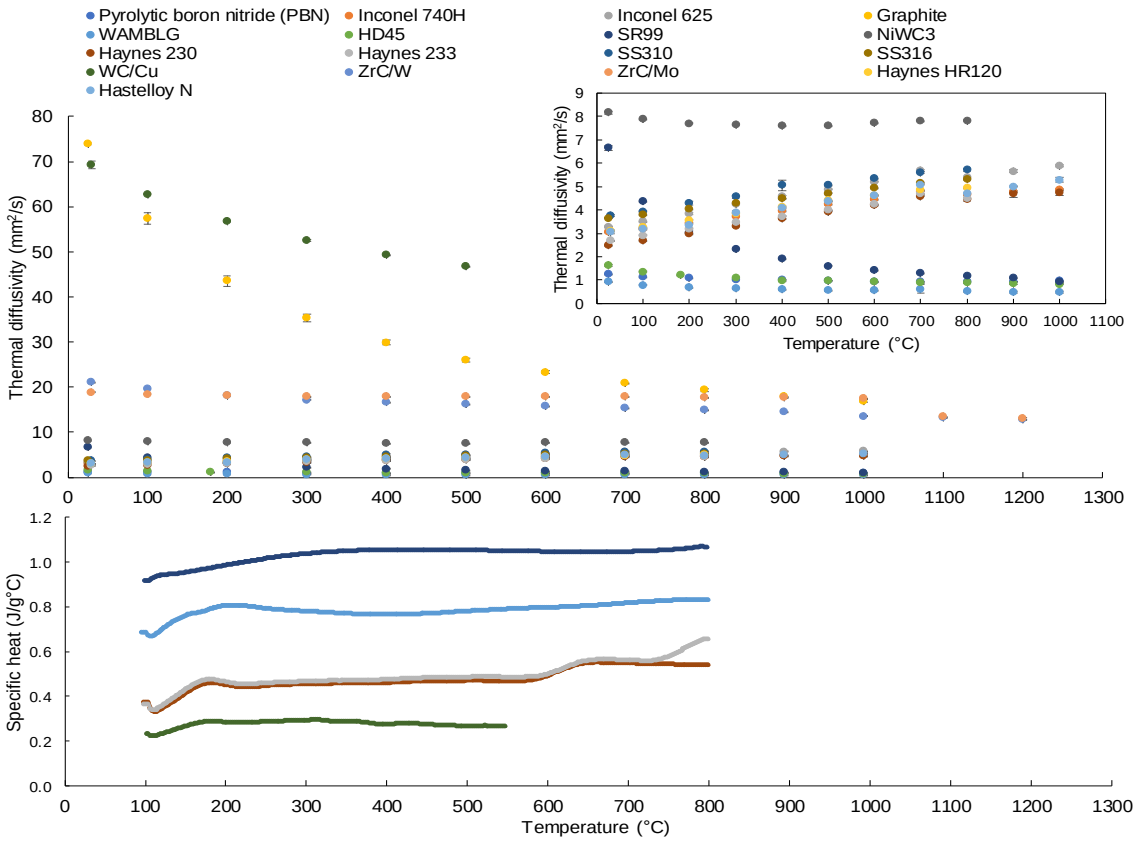

Figure 4: **A**. Temperature-dependent thermal diffusivity of all containment materials. Standard deviation bars are shown of the three shots taken per sample by the xenon lamp. The upper-right insert shows the values from 0-9 mm^2/s, where many of the metal alloys are coincident. **B**. Temperature-dependent specific heat measured for five of the containment materials.

DISCUSSION

Measured specific heat values show that the highly-alloyed CMs (Haynes 230 and 233) undergo at least one second-order phase transition at high temperatures. These disordered nickel-chromium blends have complex phase relationships; however, these clear transitions have been observed in several of the other stainless steels and nickel-alloys (data not shown), so is common to these selected refractory materials.

WC/Cu shows a relatively constant specific heat as temperature increases; a study on tungsten carbide reinforced copper composites noted that WC does not undergo a phase transition [21].

The specific heat for WAMBLG is significantly higher than the other CMs. Testing this alumina-silica blend has been technically difficult as it requires multiple annealing steps to achieve repeatable results.

The thermal diffusivity of the nickel-based alloys and stainless steels, which are majority iron, all show similar, increasing trends that have previously been fitted to linear models in the literature [22]. The two zirconium carbide blends, ZrC/W and ZrC/Mo, have curves that are significantly higher than the alloyed metals; the lab that provided these cermet test samples reports that ZrC/W has a thermal conductivity 2x-3x higher than standard iron- or nickel-based alloys at the same temperature [15].

The three insulating ceramics tested – PBN, WAMBLG, and SR99 – have the lowest measured thermal diffusivity of the entire group. And of all the materials tested, graphite has the highest measured thermal diffusivity at room temperature. The sample's curve decreases significantly with increasing temperature; this is due to the increase in phonon-phonon interactions that occur in graphite above room temperature. Above 25°C, the high frequency of scattering events causes thermal conductivity (and thermal diffusivity) to decrease [23].

CONCLUSIONS

This project involved testing the thermophysical properties of several CSP containment materials for systems operating above 700°C. These materials were selected by the CSP community and include nickel-based alloys, alumina-silica ceramics, and ceramic

metals. As of now, specific heat results for five of the sixteen CMs have been experimentally repeated; the other materials have presented difficulties in the form of excessive oxidation, sample-crucible sintering, and multiple annealing runs. Laser flash diffusivity measurements have been repeatable with single samples but will be reproduced with other samples from the same bulk material. Temperature-dependent thermal diffusivity values for the highly-alloyed metals and ceramics are consistent with the literature; understanding these properties for new ceramic metals is more complex and will be investigated in future studies.

Future work will involve testing materials that have been exposed to challenging environments, including corrosion, thermal aging, and thermal cycling.

ACKNOWLEDGMENTS

This work was supported by the U.S. Department of Energy Solar Energy Technologies Office under Award Number DE-EE0008371. We thank Scott Elliot and Nathan Mauldin of the Montgomery Machining Mall as well as Dennis Denney and Jeff Wilkie at the Georgia Tech Research Institute's Machine Services office for machining samples and helpful discussions.

REFERENCES

[1] "2014: The Year of Concentrating Solar Power." 2014. https://www.energy.gov/sites/prod/files/2014/10/f18/CSP-report-final-web.pdf.

[2] "Stainless Steel – Properties and Applications of Grades 310/310S Stainless Steel." AZO Materials. https://www.azom.com/article.aspx?ArticleID=4392.

[3] "Specification Sheet: Alloy 316/316L." Sandmeyer Steel Company. https://www.sandmeyersteel.com/images/316-316l-317l-spec-sheet.pdf

[4] "Inconel Alloy 740H A Superalloy Specifically Designed for Advanced Ultra Supercritical Power Generation." PCC Energy Group. https://www.specialmetals.com/assets/smc/documents/alloys/inconel/inconel-alloy-740-h.pdf

[5] "Inconel Alloy 625." Special Metals: A PCC Company. https://www.specialmetals.com/assets/smc/documents/alloys/inconel/inconel-alloy-625.pdf

[6] "Haynes 230 Alloy." Haynes International. http://haynesintl.com/docs/default-source/pdfs/new-alloy-brochures/high-temperature-alloys/brochures/230-brochure.pdf

[7] "Haynes 233 Alloy." Haynes International. http://haynesintl.com/docs/default-source/pdfs/new-alloy-brochures/high-temperature-alloys/brochures/233-h-3183.pdf?sfvrsn=906438d4_8

[8] "Haynes HR-120 Alloy." Haynes International. http://haynesintl.com/docs/default-source/pdfs/new-alloy-brochures/high-temperature-alloys/brochures/HR-120.pdf?sfvrsn=38b829d4_48

[9] "Hastelloy N Alloy." Haynes International. http://haynesintl.com/docs/default-source/pdfs/new-alloy-brochures/corrosion-resistant-alloys/brochures/n-brochure.pdf?sfvrsn=18

[10] "Graphite (C) – Classifications, Properties & Applications." AZO Materials. https://www.azom.com/article.aspx?ArticleID=1630

[11] "Pyrolytic Boron Nitride (PBN) Crucibles." American Elements. https://www.americanelements.com/pyrolytic-boron-nitride-pbn-crucibles-10043-11-5

[12] "SR-90, SR-99, SR-99 LS Firebrick." Morgan Advanced Materials. http://www.morganfireprotection.com/media/2980/sr-90_sr-99_sr-99_ls_firebrick.pdf

[13] "WAMBLG." Westmoreland Advanced Materials.

[14] "Tailor-made solutions for the chemical & petrochemical industry." http://www.aktec.tc/upload/Rath_Chemical_Petrochemical_Industry_en.pdf

[15] M. Caccia, M. Tabandeh-Khorshid, G. Itskos, A. R. Strayer, A. S. Caldwell, S. Pidaparti, *et al.*, "Ceramic-metal composites for heat exchangers in concentrated solar power plants," *Nature*, vol. 562, pp. 406-409, Oct 2018.

[16] Tang, Haixiong, and Joseph Hensel. "High Toughness Cermets for Molten Salt Pumps." Medium: ED; Size: 27 p.: ; Powdermet Inc., Euclid, OH (United States), 2018.

[17] Office of Energy Efficiency & Renewable Energy. n.d. "Generation 3 Concentrating Solar Power Systems (Gen3 CSP)." U.S. Department of Energy. https://www.energy.gov/eere/solar/generation-3-concentrating-solar-power-systems-gen3-csp.

[18] Shaw, T L, and J C Carrol. 1998. "Application of Baseline Correction Techniques to the 'Ratio Method' of DSC Specific Heat Determination." *International Journal of Thermophysics* 19 (6): 1671–80. https://doi.org/10.1007/BF03344918.

[19] ASTM. 2005. "Designation: E 1269-05 Standard Test Method for Determining Specific Heat Capacity by Differential Scanning Calorimetry."

[20] Parker, W. J., R. J. Jenkins, C. P. Butler, and G. L. Abbott. "Flash Method of Determining Thermal Diffusivity, Heat Capacity, and Thermal Conductivity." *Journal of Applied Physics* 32, no. 9 (1961): 1679-84.

[21] Girish, BM, Basawaraj, BM Satish, and PK Jain. "Tungsten Carbide Reinforced Copper Composites for Thermal Management Applications." *Proceedings of the Institution of Mechanical Engineers, Part L:*

Journal of Materials: Design and Applications 226, no. 4 (2012): 316-21.

[22] Hofmeister, Anne M., E.M. Criss, and A.M. Hofmeister. 2019. “Transport Properties of Metals, Alloys and Their Melts From LFA Measurements.” *Measurements, Mechanisms, and Models of Heat Transport*, January, 295–325. https://doi.org/10.1016/B978-0-12-809981-0.00009-7.

[23] Pavlov, T., L. Vlahovic, D. Staicu, R.J.M. Konings, M.R. Wenman, P. Van Uffelen, and R.W. Grimes. 2017. “A New Numerical Method and Modified Apparatus for the Simultaneous Evaluation of Thermo-Physical Properties above 1500 K: A Case Study on Isostatically Pressed Graphite.” *Thermochimica Acta* 652 (June): 39–52. https://doi.org/10.1016/J.TCA.2017.03.004.